

Early Science Result from the Japanese Virtual Observatory: AGN and Galaxy Clustering at $z = 0.3$ to 3.0 *

Yuji SHIRASAKI¹ Masahiro TANAKA¹ Masatoshi OHISHI¹ Yoshihiko MIZUMOTO¹ Naoki YASUDA² Tadafumi TAKATA¹

¹National Astronomical Observatory of Japan, 2-21-1 Osawa, Mitaka City, Tokyo, 181-8588, Japan

²The Institute for Cosmic Ray Research, University of Tokyo, 5-1-5 Kashiwa-no-Ha, Kashiwa City, Chiba, 277-8582, Japan
yuji.shirasaki@nao.ac.jp

(Received 2009 0; accepted 2009 0)

Abstract

We present the result of projected cross correlation analysis of AGNs and galaxies at redshifts from 0.3 to 3.0. We used the Japanese Virtual Observatory (JVO) to obtain the Subaru Suprime-Cam images and UKIDSS catalog data around known AGNs. We investigated $\sim 1,000$ AGNs, which is about ten times larger samples than previous studies covering the redshifts larger than 0.6. We found significant excess of galaxies around the AGNs at redshifts of 0.3 to 1.8. For the lowest redshift sample ($z < 0.8$), we obtained correlation length of $r_0 \sim 5$ Mpc, which indicates that the AGN at these redshifts resides in a similar environment to typical local galaxies. We also obtained redshift dependence of r_0 in each luminosity group, which show the AGN produced at higher redshift resides in a denser environment than the lower redshift AGN does. For AGNs at the highest redshift sample ($z > 1.8$), we could not obtain a significant clustering signature and put an upper limit of $r_0 < 17$ Mpc (90% C.L.). These results are compatible with the major merger scenario which incorporates the downsizing of mass assembly.

Key words: astronomical data bases: miscellaneous — galaxies: clusters: general — galaxies: nuclei — cosmology: large-scale structure of universe

1. Introduction

It has been believed that the origin of AGN activity is accretion of matters into a massive black hole at the center of the galaxy (e.g. Lynden-Bell 1969). In order to explain the activity of an AGN with mass $\sim 10^9 M_\odot$, a large fraction of matters in the galaxy must be delivered to the inner regions of a galaxy on a short timescale, $\ll 10^9$ yr (Hopkins et al. 2008). One possible mechanism for causing the rapid inflows of the gas into the central region is a major merger between gas-rich galaxies (e.g. Kauffmann and Haehnelt 2000). If this is the case, AGNs are expected to be found in an environment of higher galaxy density than an environment of typical galaxies. The dependencies of the AGN environment on their optical, radio, or X-ray luminosity, or on redshift have been examined in various studies. Most of the observations, however, indicate that AGNs resides in an environment comparable to typical galaxies.

Using the SDSS data, the study of the environment of AGNs at redshift < 0.6 has been carried out by several authors. Miller et al. 2003 estimated the fraction of galaxies with an AGN based on 4921 galaxies at redshifts less than ~ 0.1 . They found that the fraction of galaxies with an AGN is independent of the local galaxy density. Sorrentino et al. 2006 examined 1829 AGNs at redshift < 0.1 , and found no evidence of a relation between the

environmental properties and AGN activity. Coldwell and Lambas 2006 analyzed the environment of ~ 2000 AGNs at redshift < 0.2 , and found that the galaxy number density around the AGNs is similar to that of typical galaxies. Serber et al. 2006 analyzed the local environment of 2028 $z < 0.4$ QSOs, and found that the QSOs are located in higher density environment than are L^* galaxies and the over-density increase with decreasing scale at distances of less than 0.5 Mpc of the QSO. They also reported that there is a luminosity dependence of the density enhancement at small-scale and at the brightest end. Strand et al. 2008 investigated the relationship between the AGN environment and the type, luminosity and redshift of the AGN itself. They extends the redshift space up-to 0.6 compared to the work by Serber et al. 2006 by applying a photometric redshift cut on the galaxies to reduce the projection effects. The number of AGN samples are increased to ~ 11000 . They concluded that the AGN environment depends on the luminosity of AGNs but not on the type of AGNs (type I, type II), and that there is marginal evidence for redshift evolution of type I QSO environments.

Since the observation of galaxies by the SDSS is limited to the redshift less than ~ 0.6 , measurements of AGN environment at higher redshifts need to be carried out by an infrared instrument on a 2–4 m class telescope or an optical observation by an 8 m class telescope. Barr et al. 2003 observed environment of 21 radio-loud QSOs at $0.6 < z < 1.1$ with multiple filters of optical to near infrared bands. The observations show that the radio-loud QSOs at these redshifts exist in a wide variety of environments, from field through compact groups to rich clusters, and

* Based on data collected at Subaru Telescope, which is operated by the National Astronomical Observatory of Japan (NAOJ). Data is retrieved from the JVO (<http://jvo.nao.ac.jp/portal>) operated by the NAOJ

indicate no evidence of redshift dependence of the environments. They also found that the QSOs are not always located at the center of a galaxy group or cluster, which contrasts with low redshift clusters where QSOs reside at the center of galaxy distribution. Coil et al. 2007 measured clustering properties around 52 SDSS and DEEP2 QSOs at redshifts 0.7 – 1.4, cross-correlating each QSO with the DEEP2 galaxies. They found that the clustering scale length between the QSOs and galaxies is comparable to the scale length obtained by auto-correlation of DEEP2 galaxies, and obtained correlation length of 3.3 ± 0.7 Mpc. No significant dependence was found on luminosity or redshift. Adelberger and Steidel 2005 examined clustering property of AGN and galaxy at redshifts from 1.5 to 3.5, and dependence on the AGN optical luminosity was measured. The galaxy sample used in their analysis comes from color-selected spectroscopic targets. They divided 79 AGN samples into two luminosity groups and derived correlation lengths of 4.7 ± 2.3 Mpc and 5.4 ± 1.2 Mpc for the low and high luminosity groups, respectively. They report no evidence of luminosity dependence. Bornancini et al. 2007 examined a correlation between the 13 SDSS QSOs and the distant red galaxies (DRG) at redshifts from 1 to 2. They report correlation length of 5.4 ± 1.6 Mpc,

As introduced above, the current observations indicate that AGNs do not reside in a particularly high density environment. Dependence of the clustering strength on redshift or AGN luminosity is observed by some of the experiments, but it is still controversial. These evidences are against to the galaxy merger scenario, since the merger event is expected to happen more frequently in a denser environment than in a normal environment. There are several observational evidences that mass assembly of larger system terminates earlier than that of smaller system. From this observational fact, it is expected that at higher redshift the merger occurs in an environment of high galaxy density. Thus the AGN produced at a higher redshift should be observed in a high galaxy density environment.

We must, however, be cautious with the results obtained especially at high redshift ($z > 0.6$). All the high redshift experiments ever achieved are based on the galaxy samples selected by a color cut. The color selection utilizes the rest-frame optical break at 4,000 Å to infer the redshift, so blue galaxies which do not exhibit the prominent break feature are missed in the galaxy samples. An unbiased galaxy selection should be utilized to investigate the effect of the environment on the evolution of a massive black hole.

In this paper we present the measurements of AGN environment at redshifts from 0.3 to 3.0, which is the first scientific result obtained from the Japanese Virtual Observatory (JVO). The JVO provides reduced Subaru Suprime-Cam images which passed the proprietary period. The JVO provides the functionality that enables the multiple region search against a image data service with a single JVOQL, which is an extension of database language SQL and can describe a coordinate join between Suprime-Cam image metadata table and QSO/AGN cat-

alog table. The UKIDSS World DR2 is also used to detect distant galaxies which are dark in optical bands but bright enough to be detected in near-infrared bands. Total number of QSO/AGN samples used in this work is $\sim 1,000$. A strength of this work is the largest AGN sample with deep optical images, which are typically deeper than 24 mag. By using the deep optical images, we can also measure the clustering property of faint and blue star forming galaxies around an AGN at high redshift ($z \sim 1 - 2$), which have not well explored by any other studies. We are also almost free of the cosmic variance, since the AGNs we have used are distributed in a wide area of the sky. In that sense, our study uses a nearly unbiased galaxy sample, and it is adequate for study of the AGN environment.

2. The Datasets and Data Selection

All the data used in this work were obtained from the Japanese Virtual Observatory (JVO). The dataset accessed through the JVO are: Catalog of Quasars and Active Galactic Nuclei (12th Ed.) by Veron-Cetty et al. 2006, SDSS DR-5 Quasar Catalog (4th Ed.) by Schneider et al. 2007, Subaru Suprime-Cam Reduced Image Archive of JVO, and UKIDSS DR2 catalog by Warren et al. 2007

First we selected AGNs for which Suprime-Cam images or UKIDSS data were available for their environment analysis. We sent a query to the JVO to find AGNs at redshift of 0.3–3.0. 4638 AGNs were found to be contained in or near of the the Suprime-Cam images, and 4084 AGNs were included in the UKIDSS DR2. As a result, the total number of AGNs selected with this search was 5976.

Next, to reduce a projection effect by galaxy clustering associated with the other foreground AGNs, the AGNs which have another identified AGN at smaller redshift and within a angle corresponding to 2 Mpc at their redshift were removed from the sample. After this selection, the total number of AGNs in the sample was reduced to 4745.

Then the Suprime-Cam images and/or the UKIDSS data corresponding to each AGN were retrieved, and the uniformity of the images and data coverage for the AGN field were examined. We define the AGN field as a circular region with 2 Mpc radius centered at the AGN coordinate.

The quality of the Suprime-Cam images retrieved from the JVO is sometimes highly inhomogeneous, because the images were created by stacking multiple exposures. Some part of the image, therefore, may have significantly smaller exposure than the other part. The inhomogeneity was estimated from the distribution of RMS of the background. The RMS of the background was calculated with the SExtractor (Bertin and Arnouts 1996) at every image pixel. We removed the images for which the standard deviation of RMS over the entire AGN field was larger than 10% of the average. $\sim 30\%$ of the images were rejected with this criterion. The Suprime-Cam images which did not have photometric calibration data were also removed. $\sim 70\%$ of images had photometric calibration.

In order to examine the data coverage for the AGN field, an effective observation area was calculated for each annulus centered at the AGN coordinate. The width of

each annulus was taken to be 0.1 Mpc. The effective area was calculated by counting the effective pixels for the case of Suprime-Cam image or by counting the object number for the case of UKIDSS catalog data. The effective pixel is a pixel which has data usable for the object detection. Unobserved regions and regions illuminated by bright objects were ignored in calculating the effective area.

We imposed a requirement for the data that at least 80% of coverage at any of the annuli should be obtained. For data that did not satisfy this condition were removed. The data coverage fraction obtained here was used in estimating the galaxy number density at each annulus. After these selections, 2183 AGNs remained for further analysis.

We removed data of shallow observation based on the average number density ρ_0 of observable objects at the AGN redshift to reduce the signal to noise ratio. ρ_0 was estimated by integrating a luminosity function up to limiting magnitude m_{limit} of each image. For an actual observation, however, the detection efficiency of an object with magnitude m smoothly decreases from one to zero around m_{limit} . Thus the m_{limit} should be determined so as to satisfy the following condition:

$$\int_{m_{\text{min}}}^{m_{\text{limit}}} F_{\text{true}}(m) dm = \int_{m_{\text{min}}}^{m_{\text{max}}} F_{\text{obs}}(m) dm, \quad (1)$$

Where F_{true} is a true differential magnitude distribution not suffered from detection efficiency, and F_{obs} is an observed differential magnitude distribution. m_{min} and m_{max} are minimum and maximum magnitudes of the observed objects, respectively. As a simple estimator for m_{limit} , we measured a peak of the magnitude distribution for each image. We confirmed that the integration of $F_{\text{true}}(m)$ up to m_{limit} estimated from the peak of the distribution gives a good approximation for the total observed number of objects, where $F_{\text{true}}(m)$ was derived by fitting a power law function to the observed magnitude distribution at a 100% completeness region. We used the luminosity function obtained by Gabasch et al. (2004), Gabasche et al. (2006), and Cirasuolo et al (2007). Then the data of which ρ_0 was greater than 0.0001 Mpc^{-3} for any one of the observed bands were selected.

Finally, the AGNs of which K-corrected absolute magnitude in V or g' band were in the range from -30 to -20 were selected. After these selections described above, the total number of AGNs remained for further analysis was 963. Additional finer data selections will be made in the further analysis, which will be described in the next section, and the number AGN analyzed in this work is 747.

The celestial distribution of the 747 AGNs is shown in Figure 1. The AGNs are widely distributed in the sky, and we can expect that the effect by the cosmic variance is almost ignored in our analysis.

The numbers of AGNs samples n_{AGN} and the minimum, maximum and median value of the limiting magnitude for each AGN subset are summarized in Table 1. 23% of the sample have data of both the optical and infrared, 59% have data of optical band only, and 18% have data of infrared band only. The typical limiting magnitudes for optical and infrared bands are 24.8 and 19.6, respectively.

The Suprime-Cam images provided at the JVO were processed using the JVO Suprime-Cam reduction pipeline (version 0.1.24) which was developed based on the Suprime-cam Deep Field REDuction (SDFRED) package (Ouchi et al. 2004). The calculations were made on the JVO grid computing system (Shirasaki et al. 2008). The SDFRED is based on a software package developed for Suprime-Cam data reduction (Yagi et al. 2002).

The data were reduced in the following procedure: For each CCD frame, 1. bias subtraction, 2. flat field correction, 3. distortion correction and 4. astrometric correction were carried out. The relative positions, rotation angles, and flux normalization factors were calculated for every frame, then they were stacked to make a single mosaic frame. The photometry was performed using the data of standard star observations which were taken on the same day as one of the stacked frames were taken. From the comparison with the SDSS catalog, the differences of photometric magnitudes were less than 0.2 for 90% of the compared images. The astrometric accuracy were estimated by comparing with the USNO catalog. The peak of the distribution of angular difference to the USNO data was 0.3 arcsec and 99% were less than 1.2 arcsec.

3. Cross-Correlation Analysis

The two-point cross-correlation function ξ is generally used to measure the clustering properties between an AGN and galaxies, which is defined as:

$$\xi(r) = \rho(r)/\rho_0 - 1, \quad (2)$$

where $\rho(r)$ is the number density of galaxies at a distance r from the AGN, and ρ_0 is the average number density of galaxies at the AGN redshift. Since distances to the galaxies were not measured in this work, the projected cross-correlation function ω was compared with the observation. We assumed a power law function for the density profile around the AGN, $\xi = (r_0/r)^\gamma$.

The projected cross-correlation function is obtained by integrating the Equation 2 along the line of sight, then it is described as:

$$\omega(r_p) = r_p \left(\frac{r_0}{r_p} \right)^\gamma \frac{\Gamma(1/2)\Gamma((\gamma-1)/2)}{\Gamma(\gamma/2)}, \quad (3)$$

where r_p is a distance perpendicular to the line of sight, Γ is the Gamma function. The $\omega(r)$ averaged over a sample of AGNs was measured as:

$$\omega(r_p) = \frac{n(r_p) - n_{bg}}{\sum \rho_{i,0}/m}, \quad (4)$$

$$n(r_p) = \frac{\sum N_i(r_p)}{\sum S_i(r_p)} \quad (5)$$

where $n(r_p)$ is a projected galaxy number density averaged over m AGNs as a function of a projected distance from the AGN, $N_i(r_p)$ is the number of observed galaxies at a distance range of $r_p \sim r_p + dr$ for the i -th AGN, $S_i(r_p)$ is the projected area corresponding to the distance range, $\rho_{i,0}$ is the average number density of galaxies at the AGN

redshift. $\rho_{i,0}$ is calculated from the luminosity function obtained by Gabasch et al. (2004), Gabasche et al. (2006), and Cirasuolo et al (2007). In calculating $N_i(r_p)$, we took into account the coverage fraction for each annulus of i -th AGN, $f_i(r_p)$, as follows: For each object detected at distance r_p , we assigned a weight defined as $1/f_i(r_p)$. We calculated a sum of the weight for every distance bins, then obtained $N_i(r_p)$.

We created catalogs from each Suprime-Cam image using the SExtractor (Bertin and Arnouts 1996). In case that there were multi-band images for the examined field, the regions which were not covered by any one of the images were ignored in the object detection. For each AGN, a multi-band catalog was created by matching the Suprime-Cam single band catalogs and the UKIDSS catalog if they existed. The galaxy number count, $N_i(r_p)$, was derived from the multi-band catalog.

At near of the AGN, galaxies are contaminated by the light of the AGN, so the detection rate of the galaxies is lowered there. So, in deriving $N_i(r_p)$, a region of 4 arcsec from an AGN was masked and the data of this region was ignored. The typical FWHM of the Suprime-Cam image used in this work is less than 1 arcsec, so the effect of the AGN to the galaxy detection efficiency is negligibly small at outside of the masked region if the apparent brightness of the AGN is dimmer than 17 mag. The reduction of the projected area due to the masking was corrected when calculating $S_i(r_p)$.

The foreground cluster or group of galaxies can be a noise for the clustering analysis. To reduce the effect of the accidental alignment of the foreground cluster, the reduced χ^2 and maximum deviation σ_{max} of the galaxy density distribution were calculated at distance range of 0.5–2.0 Mpc. We also calculated a clustering coefficient B_{gg} around each AGN, which was defined as $\xi(r) = B_{gg}r^{-\gamma}$ and was calculated as:

$$B_{gg} = \frac{3 - \gamma}{2\pi} \frac{N_{total} - N_{bg}}{\rho_0} (0.3 \text{ Mpc})^{\gamma-3}, \quad (6)$$

where N_{total} is the total number of observed galaxies at $r_p < 0.3$ Mpc, and N_{bg} is the expected background count at $r_p < 0.3$ Mpc estimated from the average density at $r_p > 1$ Mpc. If foreground cluster is accidentally located at near of the AGN, significantly large B_{gg} values is observed. B_{gg} might become very large due to the actual association of a galaxy cluster with the AGN. We removed such an extreme sample, as it significantly increases the average clustering strength. The criteria used here were $B_{gg} \geq -1000$ and $B_{gg} < 1000$, $\chi^2/n \leq 2.5$ and $\sigma_{max} \leq 3.0$, and the fraction of data rejected by these criteria were $\sim 6\%$, $\sim 2\%$, and $\sim 5\%$ respectively.

4. Results

We divided all the AGN samples into four redshift ranges, $z = 0.3\text{--}0.8$, $0.8\text{--}1.5$, $1.5\text{--}1.8$, and $1.8\text{--}3.0$. For each redshift group, the dataset is further divided into a dimmer subset ($M_V \geq -25$) and a brighter subset ($M_V < -25$). In Figure 2, the absolute magnitude and redshift distribu-

tion of the AGN used in this work are shown. Hereafter we call an AGN of $M_V \geq -25$ as a dim AGN, and an AGN of $M_V < -25$ a bright AGN. The bright AGNs for $z < 0.8$ and the dim AGNs for $z \geq 1.5$ are not analyzed due to poor statistics.

For each subset, we derived a galaxy number density, $n(r_p)$, as a function of distance from the AGN, and it was fitted with a model function described in the previous section. In Figure 3, the galaxy density profile for each AGN subset is shown with solid circles, and the model function fitted to the observation is shown with a solid line. We fixed the slope parameter γ to 1.8 which is a canonical value obtained from auto-correlation analysis among typical galaxies by any other works. The fitting parameters are summarized in Table 2.

Evidence of galaxy clustering around the AGNs was detected in 90% confidence level for all the datasets except for the dataset of the highest redshift. We derived correlation lengths of 6.3 ± 0.6 Mpc, 9.5 ± 1.3 Mpc, 4.5 ± 1.8 Mpc, and 14.1 ± 2.1 Mpc, for $z = 0.3\text{--}0.8$ (Dark), $z = 0.8\text{--}1.5$ (Dark), and $z = 0.8\text{--}1.5$ (Bright), and $z = 1.5\text{--}1.8$ (Bright), respectively. For datasets of $z = 1.8\text{--}3.0$ (Bright), no significant clustering signature was observed, and we derived upper limits of the correlation length as 17 Mpc in 90% C.L..

To evaluate the systematic effect we examined eight independent offset fields for the dataset of $z = 1.5\text{--}1.8$ (Bright). The offset fields were apart from each AGN by 4 Mpc to directions of right ascension and/or declination axis. We applied them the same procedure adopted on the AGN dataset. The right bottom panel of the Figure 3 shows the density distribution at the offset positions, which was obtained by taking an average over one of the eight offset fields that satisfied the criteria adopted to the AGN dataset. No systematic excess was seen for the offset field.

We also derived density distributions averaged over each of the eight offset fields. The significance of excess density at $r = 0\text{--}1$ Mpc over the average density for $r = 1\text{--}2$ Mpc are from -1.54σ to 1.42σ , while the significance of the AGN dataset was 4.8σ . As no significant systematic excess was seen for the offset fields, we conclude that the excess seen for AGN dataset is due to galaxies associated with the AGN.

The correlation length obtained for each dataset are plotted as a function of redshift (Figure 4). For a comparison, observation and simulation results of AGN-galaxy correlation analysis by the other authors are shown in the figures. Results for galaxy-galaxy auto-correlation analysis by several authors are also shown to compare the environment of the AGN with those of several types of galaxy. The bright AGN samples are shown as solid circles, and the dim AGN samples are shown as solid triangles. The upper limits is shown for the highest redshift sample.

The result for $z = 0.3\text{--}0.8$ (Dark) is consistent with the existing measurements (Hickox et al. 2009, Norman et al. 2009), which supports the validity of our analysis method. Norman et al. 2009 measured the projected cross correlation between 420 QSOs and 4975 luminous red galax-

ies (LRG) at redshifts from 0.2 to 0.8 (a square in the Figure 4) based on the data of 2QZ and 2SLAQ survey. Our measurement at $z = 0.3 - 0.8$ agrees with their value, although our value is for the correlation between AGNs and all the type of galaxies detected in the Suprime-Cam and UKIDSS survey. Hickox et al. 2009 also measured the cross correlation for three types of AGNs (asterisks in Figure 4; from top to bottom radio AGN, X-ray AGN, and IR AGN) with galaxies based on the AGN and Galaxy Evolution Survey (AGES) and Bootes multi-wavelength survey. Their sample contains 598 AGNs at redshift 0.25 - 0.8. Our result are consistent with their result for radio AGN and X-ray AGN, and slightly higher than that of their IR AGN. The clustering of local galaxies measured by Ma et al. 2009 (K-band selected galaxy), Zahavi et al. 2005 (r-band selected galaxy), and Hawkins et al. 2003 (b_J -band selected galaxy) are 5-7 Mpc (diamonds in Figure 4). Our value for AGN-galaxy correlation length are almost the same as the auto-correlation length of the local galaxies.

Our result for $z = 0.8-1.5$ (Dark) is significantly larger than the result by Coil et al. 2007. Coil et al. 2007 measured quasar-galaxy cross correlation length based on the SDSS and DEEP2 survey for 52 QSOs at redshifts from 0.7 to 1.4 (a triangle in Figure 4). The range of absolute magnitude used in Coil et al. 2007 is from -26 to -20 , which is almost equivalent to our dim AGN sample. Coil et al. 2007 measure the correlation length using the data of distance scale from 0.1 to 10 Mpc, and they introduced γ as a free parameter then obtained 1.55. Thus we fit the model function to our data of 0.1 to 2 Mpc with a fixed γ of 1.55. Then we obtained much higher correlation length of 15.4 ± 4.1 , so our result is inconsistent with the result by Coil et al. 2007. The difference may come from the difference of the used galaxy sample. DEEP2 galaxies samples are selected by a color cut, and may contains more redder galaxies than in our sample. It is also possible that the difference is due to the cosmic variance, as the number of well separated fields are only four for the DEEP2 dataset. The correlation length obtained for our dataset is almost comparable with the auto-correlation length of Luminous Red Galaxies (LRG) by Wake et al. 2008.

Our bright AGN dataset at the same redshift shows marginal evidence of the galaxy clustering, which gives smaller correlation length than the dim AGN dataset. This result indicates the existence of luminosity dependence for the AGN and galaxy clustering at this redshift range.

The density profile of the bright AGN at redshift 1.5-1.8 shows relatively flat distribution at <1 Mpc. A centralized signature is not evident, which indicates that the AGN are not located at the center of galaxy group but distributed at a scale of 1 Mpc. Thus it may not adequate to represent the clustering property with the model parameter which assume a centralized density profile. Bornancini et al. 2007 examined a correlation between the 13 SDSS QSOs and the distant red galaxies (DRG; $J - K_s > 2.3$) at redshifts from 1 to 2 (a circle in Figure 4). Their AGN samples has similar luminosity distribution to that of our

sample. They report correlation length of 5.4 ± 1.6 Mpc, which is smaller than ours. The density profile measured by them shows a power law profile, and no flattening as observed in our samples at $r_p = 0.5-1.0$ Mpc is seen. The galaxy populations used in their analysis are different from ours, so the inconsistency of the two results may be attributed to the difference of the galaxy population. The cosmic variance may again apply to the result by Bornancini et al. 2007, as they use observation data taken at a single field.

For dataset at redshift 1.8-3.0, we couldn't find any evidence of clustering signature. At these high redshifts, the number of galaxies which are brighter than the limiting magnitude is very poor and the clustering signal easily disappear due to the foreground galaxies. We obtained upper limit of 17 Mpc in 90% C.L..

5. Discussion

We show that the dim AGNs at redshift 0.3-0.8 have similar clustering properties to the typical local galaxies. If there is a correlation between the clustering properties and the mass of the dark matter halo as suggested by many simulation results, this implies that these AGNs are located in a dark matter halo which has similar mass to that occupied by typical galaxies at the local universe. We also show that the dim AGNs at redshift 0.8-1.5 and bright AGNs at redshift 1.5-1.8 have relatively denser environment than typical galaxies, while the bright AGN at redshift 0.8-1.5 have comparable or sparser environment. This result indicates that there exists redshift dependence for the environment of bright AGNs, that is, at higher redshift bright AGNs are located in a high density region, while at lower redshift they are located in a lower density region. This redshift dependence may be explained by the downsizing of the mass assembly as a following picture:

First we assume that the AGN appears as a result of galaxy major merger event which occurs during the collision of two clusters or groups of galaxies. The AGN is brightest at the early phase of its lifetime. After a while, the AGN becomes dimmer due to the decrease of the matter flow into the central black hole. At higher redshifts, assembly of larger system frequently occurs, and the collisions of larger clusters are dominated over the collision of smaller system. Thus the bright AGNs are produced in a higher density environment at the redshifts. The mass assembly of the larger system terminates earlier than the smaller system, and smaller scale assembly still proceeds at a later epoch. The AGN produced through the galaxy merger during the lower-mass assembly has high luminosity, but its environment is sparser than the environment of the AGN produced in a epoch when the larger scale mass assembly was still active.

The environment of the dimmer AGN reflects the environment where the AGN is produced, which may evolves as the calculation by Kauffmann and Haehnelt 2002 as shown in the figure 4. So the redshift dependence of the environment for the dimmer AGN follows the dependence for the bright AGN but it is shifted by a time correspond-

ing to the life time of the bright phase of AGN.

Our observational result can be explained with this framework in qualitatively. This picture also explains the flat profile of galaxy number density obtained for the bright AGNs of redshift 1.5–1.8. The flattening at $r=0.5$ –1.0 Mpc are attributed to the location of a galaxy merger, which is expected to take place at a random region of two colliding clusters. When it becomes dim, the mass assembly is almost terminated and the galaxies with an AGN fall into the center of mass gravity. Thus the galaxy distribution around the dim AGN shows a centralized profile.

Considering that there exists evidence of luminosity dependence for the AGN environment as indicated from the result for redshift 0.8–1.5, the life time of the bright phase of AGN should not be shorter than the time scale corresponding to the redshift interval, that is a few Gyr.

To be more confident about this picture, more observational data should be obtained in both quantitatively and qualitatively. The current statistic is not enough for deriving definite conclusions. It is also necessary to consider the AGN properties at other wavelengths such as X-ray, radio, and so on, since some of the AGNs are hidden in a dust or accretion disk, so their activity can not measured only from the optical luminosity. To ensure the validity of the relatively larger correlation length obtained for redshift 0.8–1.8, statistics should be enlarged by factor of ten or so, or it is necessary to remove the foreground galaxies by applying the photometric redshift technique to enhance the signal to noise ratio.

6. Conclusions

Using the Japanese Virtual Observatory, we are able to measure the clustering property for ~ 1000 AGNs at redshifts 0.3–3.0 with optical brightness of $M_V = -30$ to -20 . We divided the AGN samples into four redshift intervals and two brightness ranges.

We found significant evidence of clustering for dim AGN samples of redshift 0.3–1.5, and a bright AGN sample of redshift 1.5–1.8. The correlation lengths between the AGN and galaxies are measured for each data subset. We find that the correlation length is larger at higher redshift when compared in the same absolute brightness group. We also found that the correlation length is larger for the dim sample at redshift 0.8–1.5, so there exists luminosity dependence of the AGN environment at the same redshift. It is surprise that the dim AGNs have denser environment than the bright AGNs from the view point of galaxy merger scenario which has been introduced to explain the fueling mechanism of an AGN. It can be explained, however, by considering the downsizing of the mass assembly.

At higher redshift assembly of the larger systems are dominant over the assembly of the smaller system, so the AGN produced in this epoch has a denser environment. The assembly of the larger system terminates more rapidly than the smaller system, so the smaller scale assembly becomes dominant at lower redshift. The AGN produced during the epoch of low-mass assembly has sparser envi-

ronment than the AGN produced in the epoch of high-mass assembly. Both of the AGNs have similar brightness when it is produced, since the origin of the fueling source are galaxy merger and no quantitative difference for them may does not exist. The bright phase of an AGN terminates after a few Gyr, after that it will be observed as a dim AGN or other type of galaxies, therefore the environment of the dim AGN reflects the environment of bright AGN at higher redshift.

According to this scenario, the observed redshift dependence of the correlation length reflects the history of mass assembly. It is expected from this work that the larger system assembly is already terminated around $z \sim 1.5$, and smaller scale mass assembly, which may be still progress in the local universe, is dominated.

To be more confident about this scenario, more observational data should be obtained in both quantitatively and qualitatively. The observations of huge number of AGN fields with the Hyper Suprime-Cam, which will be installed on the Subaru telescope around 2011, will gives more definite observational evidence on the evolution of a massive black hall.

Acknowledgments

This work was supported by the JSPS Core-to-Core Program and Grant-in-aid for Information Science (15017289, 16016292, 18049074 and 19024070) carried out by the Ministry of Education, Culture, Sports, Science and Technology (MEXT) of Japan. YS is grateful for support under Grant-in-aid for Young Scientists (B) (17700085) carried out by the MEXT of Japan.

References

- Lynden-Bell D., 1969, *Nature*, 223, 690
- Hopkins, P.F., Hernquist, L., Cox, T.J., and Keres, D., 2008, *ApJS*, 176, 356
- Kauffmann, G., and Haehnelt, M. G., 2000, *MNRAS*, 311, 576
- Kauffmann, G., and Haehnelt, M. G., 2002, *MNRAS*, 332, 529
- Miller, C. J. et al., 2003, *ApJ*, 597, 142
- Sorrentino, G., Radovich M., and Rifatto A., 2006, *A&A*, 451, 809
- Coldwell, G. V. and Lambas, D. G., 2006, *MNRAS*, 371, 786
- Serber, W., Bahcall, N., Menard, B., and Richards, G., 2006, *ApJ*, 643, 68
- Strand, N. E., Brunner, R. J. and Myers, A. D., 2008, *ApJ*, 688, 180
- Barr, J. M., Bremer, M. N., Baker, J. C. and Lehnert, M. D., 2003, *MNRAS*, 346, 229
- Coil, A. L. et al., 2007, *ApJ*, 654, 115
- Adelberger, K. L., and Steidel, C. C., 2005, *ApJ*, 630, 50
- Veron-Cetty, M.-P. and Veron, P. *Astronomy and Astrophysics*, Volume 455, Issue 2, August IV 2006, pp.773-777
- Schneider, D. P. et al., 2007 *AJ*, 134, 102
- Warren, S. J. et al., 2007, arXiv:astro-ph/0703037
- Bertin, E. and Arnouts, S., 1996, *A&AS*, 117, 393
- Yagi, M. et al., 2002, *AJ*, 123, 66
- Ouchi, M. et al., 2004, *ApJ*, 611, 660
- Shirasaki, Y. et al., 2008, *Fusion Engineering and Design*, 83, 438
- Gabasch, A. et al., 2004, *A&A*, 421, 41
- Gabasch A. et al., 2006, *A&A*, 448, 101
- Cirasuolo, M. et al., 2007, *MNRAS*, 380, 585
- Bornancini, C. G. and Lambas, D. G., 2007, *MNRAS*, 377, 179
- Norman, D. J., Propris, R. De, and Ross, N. P., 2009, *ApJ*(accepted for publication), arXiv:0901.4733
- Hickox, R. C. et al., 2009, arXiv:0901.2359
- Ma, B. et al., 2009, *Research in Astronomy and Astrophysics* (accepted for publication), arXiv:0905.4361v1
- Zehavi, I., et al., 2005, *ApJ*, 630, 1
- Hawkins, E., et al., 2003, *MNRAS*, 346, 78
- Wake, D. A., et al., 2008, *MNRAS*, 391, 1674
- Kashikawa, N., et al., 2006, *ApJ*, 637, 631

Table 1. Statistics of each dataset grouped according to the wavelength coverage

Band	n_{AGN}^*	m_{min}^\dagger	m_{max}^\ddagger	m_{med}^\S
OPT and IR	172	19.4	26.9	24.6
OPT only	440	21.0	27.2	24.8
IR only	135	18.5	22.5	19.6

* Number of AGN

† minimum limiting magnitude

‡ maximum limiting magnitude

§ median limiting magnitude

Table 2. Result of the projected cross correlation analysis

z	\bar{z}^*	$M_{V,g'}^\dagger$ mag	n_{AGN}^\ddagger	r_0^\S Mpc	γ^\parallel	$n_{bg}^\#$ Mpc^{-2}	$\overline{\rho_0}^{**}$ Mpc^{-3}
0.3 – 0.8	0.55	–25.0 – –20.0	254	6.28 ± 0.64	1.8	162.4 ± 0.39	0.0134
0.8 – 1.5	1.02	–25.0 – –20.0	82	9.49 ± 1.34	1.8	161.2 ± 0.69	0.0090
0.8 – 1.5	1.20	–30.0 – –25.0	186	4.52 ± 1.79	1.8	137.7 ± 0.41	0.0061
1.5 – 1.8	1.64	–30.0 – –25.0	105	14.07 ± 2.06	1.8	138.8 ± 0.56	0.0037
1.8 – 3.0	2.15	–30.0 – –26.0	120	< 17.0	1.8	160.7 ± 1.13	0.0024

* average redshift

† K-corrected absolute magnitude range

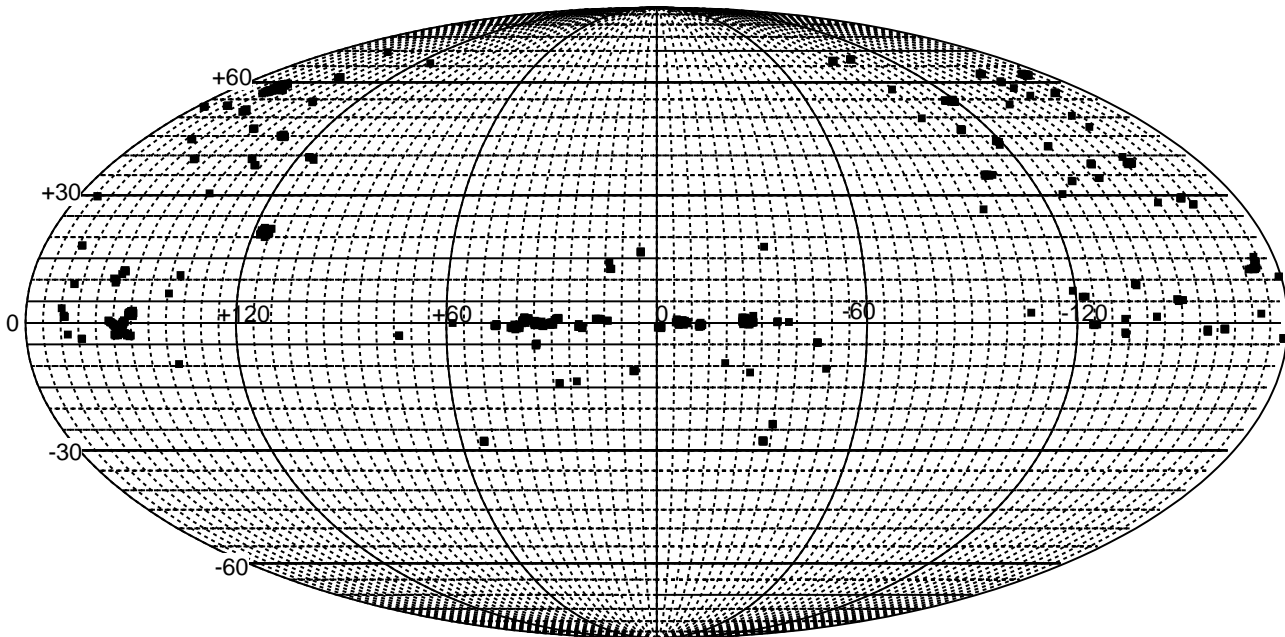
‡ number of AGNs

§ correlation length

|| slope parameter of power law density profile

projected galaxy number density for background

** average galaxy number density at the AGN redshift

**Fig. 1.** The distribution of the AGNs analyzed in this work. The coordinates are in equatorial.

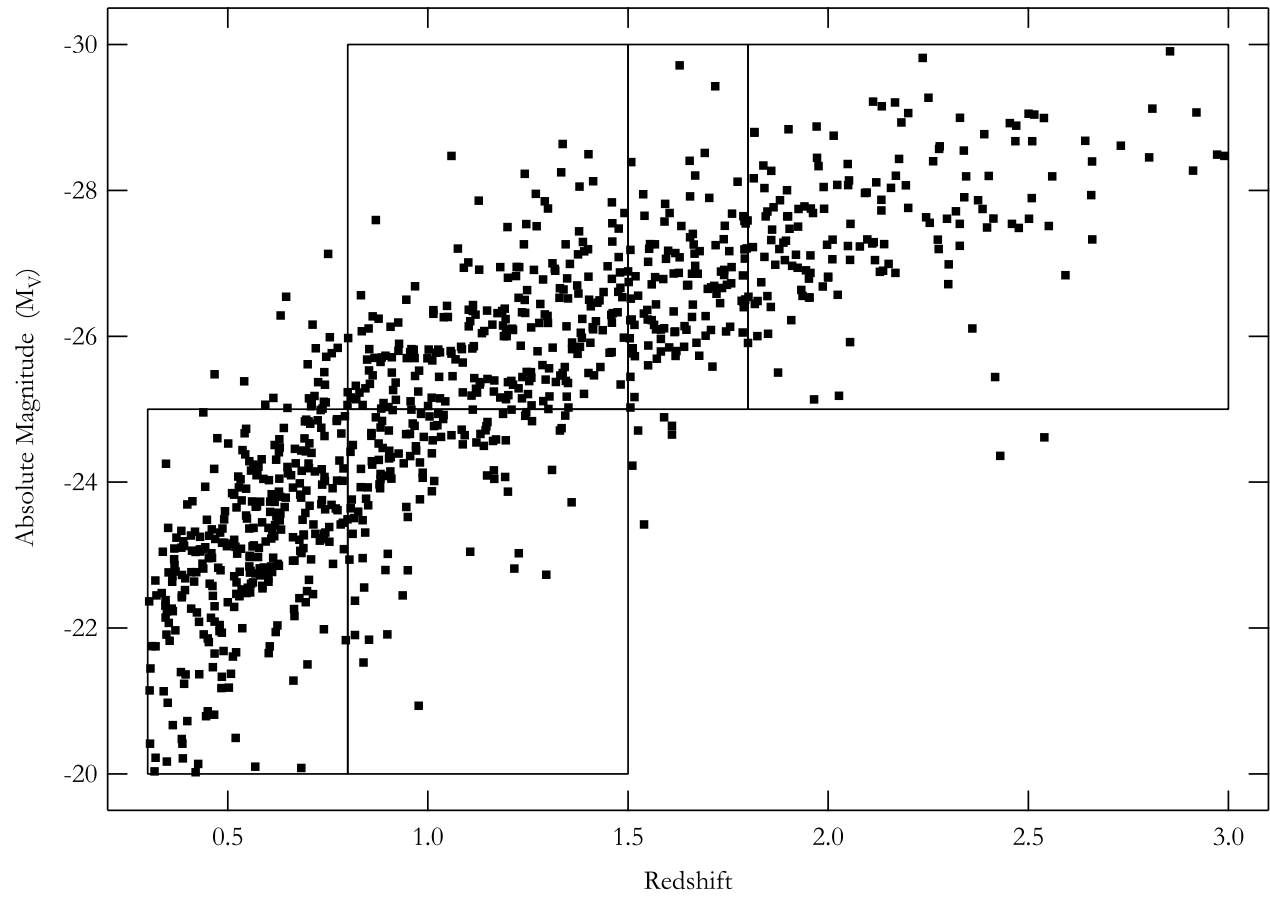


Fig. 2. K-corrected V or g' band absolute magnitude vs redshift of the AGNs used in this work.

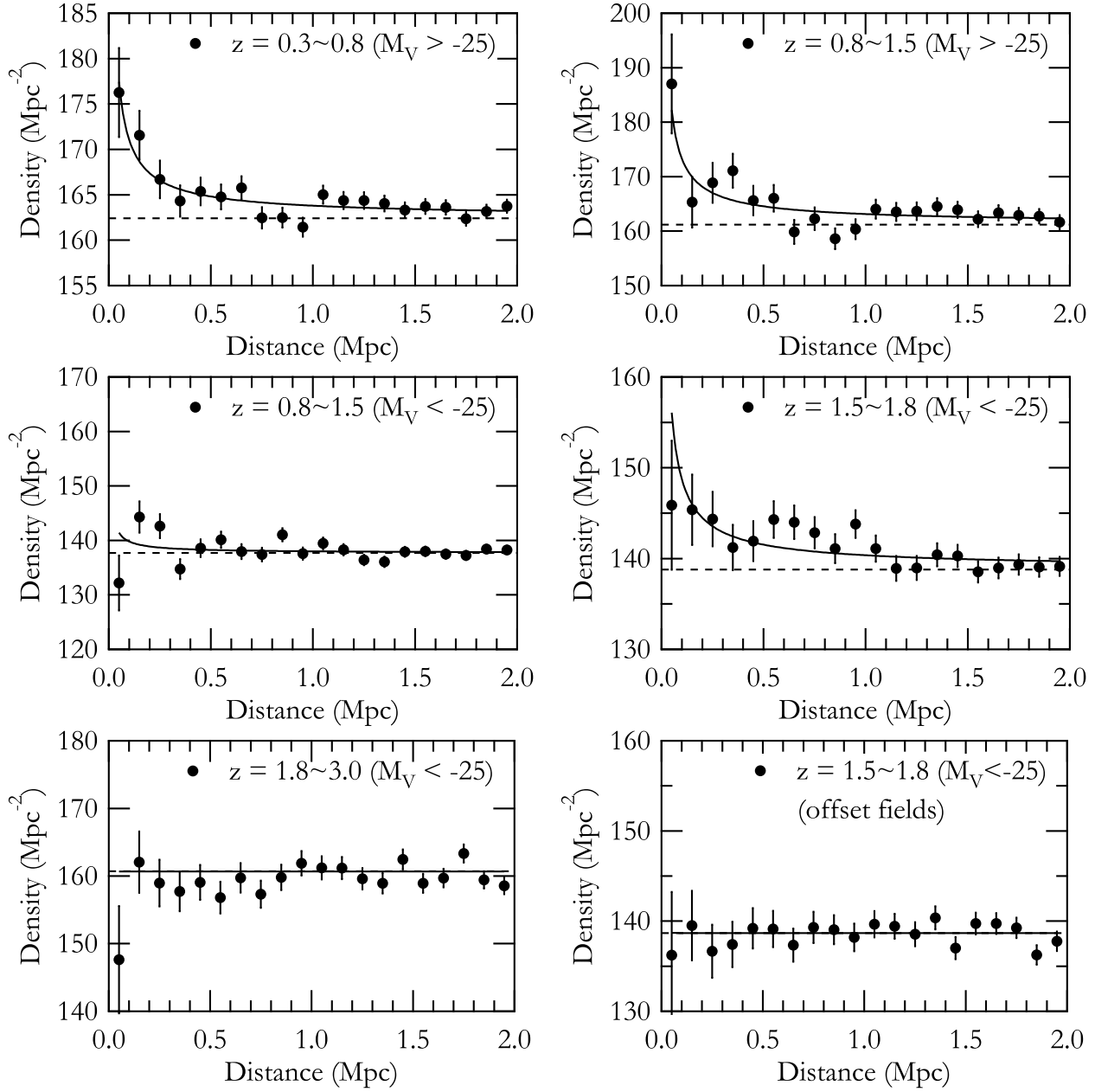


Fig. 3. Averaged galaxy number density as a function projected distance from the AGN for each redshift and brightness group. The right bottom panel is for offset field of bright AGNs of $z=1.5\text{--}1.8$.

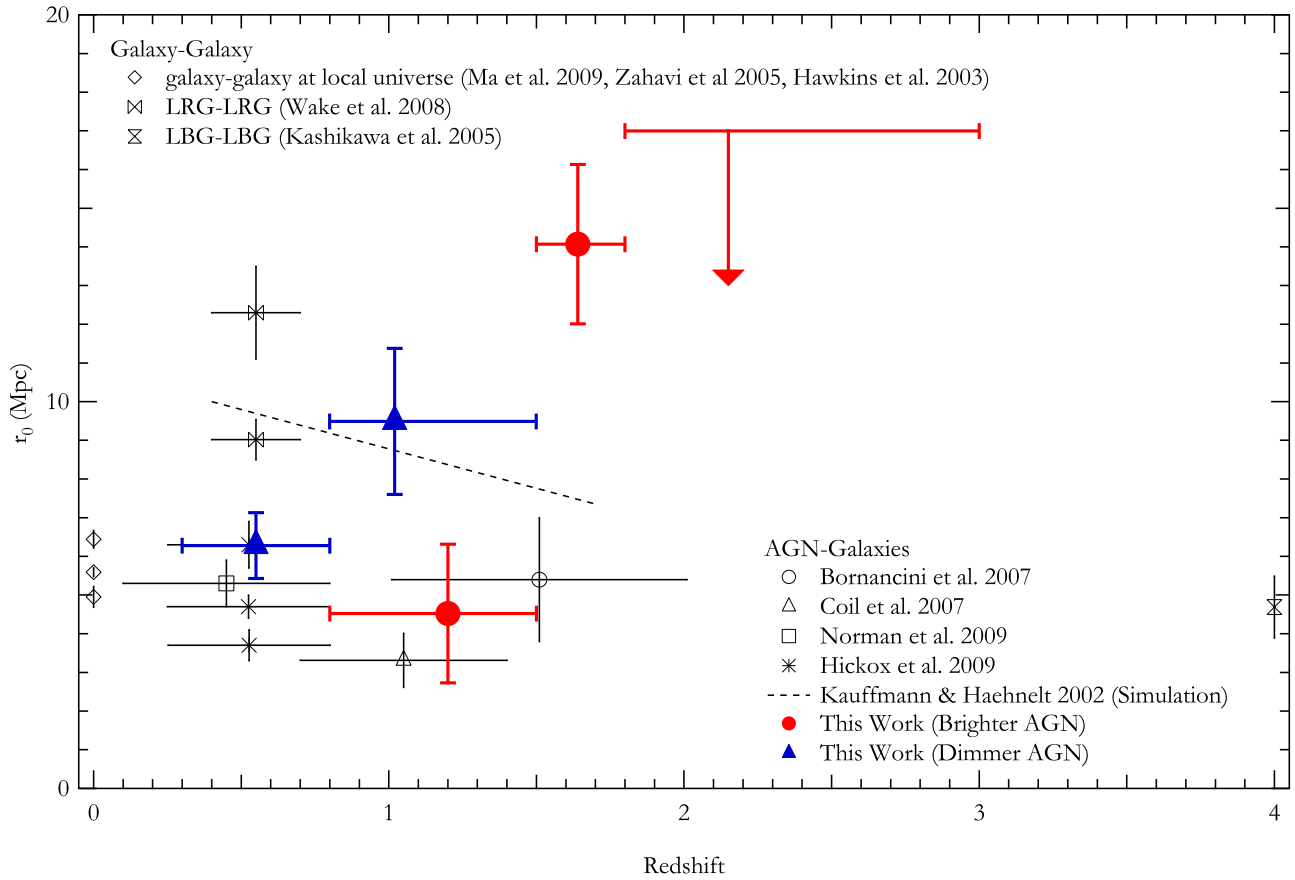


Fig. 4. Measured correlation length, r_0 , as a function of redshift.